

Formation of the η_c in Two-Photon Collisions at LEP

The L3 Collaboration

Abstract

The two-photon width $\Gamma_{\gamma\gamma}$ of the η_c meson has been measured with the L3 detector at LEP. The η_c is studied in the decay modes $\pi^+\pi^-\pi^+\pi^-$, $\pi^+\pi^-K^+K^-$, $K_S^0K^\pm\pi^\mp$, $K^+K^-\pi^0$, $\pi^+\pi^-\eta$, $\pi^+\pi^-\eta'$, and $\rho^+\rho^-$ using an integrated luminosity of 140 pb^{-1} at $\sqrt{s} \simeq 91\text{ GeV}$ and of 52 pb^{-1} at $\sqrt{s} \simeq 183\text{ GeV}$. The result is $\Gamma_{\gamma\gamma}(\eta_c) = 6.9 \pm 1.7\text{ (stat.)} \pm 0.8\text{ (sys.)} \pm 2.0\text{ (BR) keV}$. The Q^2 dependence of the η_c cross section is studied for $Q^2 < 9\text{ GeV}^2$. It is found to be better described by a Vector Meson Dominance model form factor with a J-pole than with a ρ -pole. In addition, a signal of 29 ± 11 events is observed at the χ_{c0} mass. Upper limits for the two-photon widths of the χ_{c0} , χ_{c2} , and η'_c are also given.

Submitted to *Phys. Lett.*

Introduction

The study of resonance formation via two-photon interactions in e^+e^- colliders provides valuable information on the quark substructure of the meson. The cross section for two-photon resonance formation $e^+e^- \rightarrow e^+e^-\gamma^*\gamma^* \rightarrow e^+e^-R$, where R is a $C=+1$ meson, is given by [1]

$$\sigma(e^+e^- \rightarrow e^+e^-R) = \int \sigma_{\gamma\gamma \rightarrow R} dL_{\gamma\gamma}(W^2), \quad (1)$$

with the Breit-Wigner cross section

$$\sigma_{\gamma\gamma \rightarrow R}(W^2, q_1^2, q_2^2) = 8\pi(2J_R + 1)\Gamma_{\gamma\gamma}(R)F^2(q_1^2, q_2^2) \cdot \frac{\Gamma_R}{(W^2 - M_R^2)^2 + M_R^2\Gamma_R^2}. \quad (2)$$

Here, W is the two-photon centre of mass energy, q_1^2 and q_2^2 are the squares of the virtual photon four-momenta, and $L_{\gamma\gamma}(W^2)$ is the two-photon luminosity function. The resonance R is characterised by the mass M_R , total spin J_R , total width Γ_R and the two-photon partial width $\Gamma_{\gamma\gamma}(R)$. The two-photon width and the transition form factor $F^2(q_1^2, q_2^2)$ are the two parameters to be measured.

In two-photon collisions, the scattered electron and positron emerge with a small energy loss and an almost unmodified direction after having radiated one photon each. They therefore usually go undetected along the beam direction, allowing the photons to be considered as ‘quasi-real’, with $q^2 \simeq 0$. At $q_1^2 \simeq q_2^2 \simeq 0$, the form factor $F^2(q_1^2, q_2^2)$ is normalised to unity, leaving the two-photon width as the only unknown parameter, linearly proportional to the total cross section:

$$\sigma(e^+e^- \rightarrow e^+e^-R) = \kappa \Gamma_{\gamma\gamma}(R). \quad (3)$$

If the scattered electron or positron is detected at small angles, the event is said to be *tagged*: one photon has $Q^2 = -q^2$ while the other is quasi-real with $q^2 \simeq 0$. Using tagged events, the transition form factor can be measured. It is parametrised in the Vector Meson Dominance (VMD) model by a pole form

$$F(Q^2) = \frac{1}{1 + Q^2/\Lambda^2} \quad \text{with} \quad \Lambda^2 = M_V^2, \quad V = \rho, \omega, \phi, J\dots \quad (4)$$

In the case of charmonium ($c\bar{c}$) mesons, the J^{PC} states accessible in quasi-real two-photon reactions are 0^{-+} , 0^{++} and 2^{++} , corresponding to $\eta_c(2979)$, $\chi_{c0}(3417)$ and $\chi_{c2}(3556)$. The formation of the $\chi_{c1}(3510)$, a 1^{++} state, is forbidden for two real photons according to the Landau-Yang theorem [2]. The radial recurrence $\eta'_c(3594)$ has been observed by the Crystal Ball experiment [3] in the process $\psi' \rightarrow \gamma\eta'_c$, but not in two-photon collisions [4].

In this paper we report on the study of the formation of the η_c . The two-photon width and the Q^2 dependence of the cross section are determined. Theoretical calculations, based on the assumption that the two heavy charm quarks are bound together by a QCD potential, predict 3 - 9 keV for the η_c two-photon width [5]. The Q^2 dependence of the cross section has also been calculated [6, 7]. It contains information about the quark momentum distribution inside the meson, and its shape is predicted to be well described by a VMD model form factor with $M_V = M_J$. The Q^2 dependence of the η_c cross section has not been measured up to now.

We report results from the data obtained with the L3 detector at centre of mass energies $\sqrt{s} \simeq 91$ GeV, with a total integrated luminosity of 140.2 pb^{-1} , and at $\sqrt{s} \simeq 183$ GeV, with an integrated luminosity of 52.4 pb^{-1} . This data sample includes the 30 pb^{-1} which we used

for our previous measurement of $\Gamma_{\gamma\gamma}(\eta_c)$ [8]. Since the η_c resonance does not have a dominant decay mode, nine different decay modes with branching ratios ranging from 0.5% to 2% have been analysed. They are listed in Table 1 together with the branching ratio of each channel, derived from Reference [9].

L3 detector and Monte Carlo

A detailed description of the L3 detector can be found in Reference [10]. The analysis described in this paper is mainly based on the central tracking system and the high resolution electromagnetic calorimeter.

Particles scattered at small angles are measured by the luminosity monitors (LUMI), covering a polar angle range $26 \text{ mrad} < \theta < 65 \text{ mrad}$ on each side of the detector. For data at $\sqrt{s} \simeq 183 \text{ GeV}$, particles can also be detected by the very small angle tagger (VSAT) covering a polar angle range between $5 \text{ mrad} < \theta < 8 \text{ mrad}$ for an azimuthal angle range of $-0.8 \text{ rad} < \phi < 0.8 \text{ rad}$ or $\pi - 0.8 \text{ rad} < \phi < \pi + 0.8 \text{ rad}$ [11].

The two-photon events are collected predominantly by a track trigger [12] which requires at least two charged particles with transverse momentum $p_t > 150 \text{ MeV}$, back to back, in the plane transverse to the beam, within $\pm 41^\circ$ for data at $\sqrt{s} \simeq 91 \text{ GeV}$, and within $\pm 60^\circ$ for data at $\sqrt{s} \simeq 183 \text{ GeV}$. In addition, there is a trigger for electron tags, which requires an energy deposit of at least 70% of the beam energy in the LUMI, in coincidence with at least one charged track in the central tracker.

In order to compute the acceptance and efficiency of the detector we have used the PC Monte Carlo [13], based on the formalism of Budnev *et al.* [1]. The Q^2 dependence of the cross section is taken into account using a VMD model form factor.

The particles produced in the reaction are followed through the different L3 subdetectors with the GEANT [14] simulation program and the events are reconstructed and analysed in the same way as real data.

Selection criteria

The η_c decays, listed in Table 1, result in final states with either two or four charged tracks with charge balance, accompanied by zero, one, two or four photons.

A track must have at least 18 out of a maximum of 62 hits in the central tracker. The distance of closest approach to the beam line in the transverse plane is required to be less than 3 mm, except for tracks associated with a K_s^0 decay. In order to remove electrons, we require for tracks with a momentum p larger than 0.8 GeV that $E/p < 0.9$, where E is the associated energy in the electromagnetic calorimeter.

A photon candidate is an electromagnetic cluster separated from all tracks by at least 100 mrad in ϕ and 140 mrad in θ . In the search for π^0 candidates, the two photons must both have an energy of at least 50 MeV. To reduce the combinatorial background under the π^0 signal, the angle $\psi_{\gamma\gamma}$ between the photons of the π^0 candidate must satisfy $\cos \psi_{\gamma\gamma} > 0.6$. The effective mass of the two photons must be within 20 MeV of the π^0 mass if both photons are in the barrel part of the electromagnetic calorimeter ($42^\circ < \theta < 138^\circ$), and within 30 MeV otherwise. The π^0 signal is shown in Figure 1a and 1b. The two photons of an η candidate must have an energy of at least 100 MeV, and at least one of them must be in the barrel. In addition, it is

required that $\cos \psi_{\gamma\gamma} > -0.7$, and that the $\gamma\gamma$ effective mass is within 45 MeV of the η mass, see Figure 1c.

If a cluster with at least 70% of the beam energy is found in the LUMI calorimeter or a cluster with more than 50% of the beam energy is found in the VSAT, the event is classified as tagged.

To ensure that no final state particle of the resonance decay has escaped detection, the squared vectorial sum of the transverse momenta of all detected particles, $(\Sigma \vec{p}_t)^2$, is required to be smaller than 0.1 GeV². If a tag is found, it is also included in this sum. However, if the $(\Sigma \vec{p}_t)^2$ excluding the tag is smaller than the $(\Sigma \vec{p}_t)^2$ with the tag included, the event is considered as untagged. Additionally, for events with one or more photons in the final state, the $(\Sigma \vec{p}_t)^2$ excluding the photon(s) should be larger than 0.005 GeV².

Additional cuts for each decay mode are listed below. The masses of the intermediate states which are used in the cuts are taken from the observed central values of the peaks.

$\eta_c \rightarrow \pi^+\pi^-\pi^+\pi^-$ or $\pi^+\pi^-\text{K}^+\text{K}^-$

These events leave four tracks and no photons in the detector. Using the dE/dx measurement in the central tracking system, a χ^2 to be a pion or kaon can be calculated for each track, and thus a combined probability that the four tracks are $\pi^+\pi^-\pi^+\pi^-$, $\text{K}^+\text{K}^-\pi^+\pi^-$, or $\text{K}^+\text{K}^-\text{K}^+\text{K}^-$ can be derived. For a $\pi^+\pi^-\pi^+\pi^-$ event, the $\pi^+\pi^-\pi^+\pi^-$ probability divided by the sum of $\pi^+\pi^-\pi^+\pi^-$, $\text{K}^+\text{K}^-\pi^+\pi^-$, and $\text{K}^+\text{K}^-\text{K}^+\text{K}^-$ probabilities must be larger than 55%. For a $\text{K}^+\text{K}^-\pi^+\pi^-$ event, the $\text{K}^+\text{K}^-\pi^+\pi^-$ probability divided by the sum of $\pi^+\pi^-\pi^+\pi^-$, $\text{K}^+\text{K}^-\pi^+\pi^-$, and $\text{K}^+\text{K}^-\text{K}^+\text{K}^-$ probabilities must be larger than 55%. Events that do not fall in either category are rejected. The dE/dx measurement has a good π/K separating power for tracks with a momentum $p < 0.5$ GeV. As the momenta of the decay particles of the η_c extend to 2 GeV, there exists some misidentification, which is estimated using Monte Carlo. Out of all $\eta_c \rightarrow \pi^+\pi^-\pi^+\pi^-$ Monte Carlo events that are selected, 21% are identified wrongly as $\text{K}^+\text{K}^-\pi^+\pi^-$, and of all $\eta_c \rightarrow \text{K}^+\text{K}^-\pi^+\pi^-$ Monte Carlo events that are selected, 8% are wrongly identified as $\pi^+\pi^-\pi^+\pi^-$.

$\eta_c \rightarrow \text{K}_s^0\text{K}^\pm\pi^\mp$

For this final state the geometrical reconstruction of the secondary vertex $\text{K}_s^0 \rightarrow \pi^+\pi^-$ requires two oppositely charged tracks, each with a radial distance from the interaction point in the transverse plane greater than 1 mm. The two tracks must form a secondary vertex more than 3 mm away from the interaction point. The angle between the tracks must be smaller than 2.5 rad. If the angle between the K_s^0 line of flight and the sum of the two track momenta is greater than 60 mrad, the K_s^0 candidate is rejected. Finally, the invariant mass of the two pions must be within 30 MeV of the K_s^0 mass, see Figure 1d.

$\eta_c \rightarrow \pi^+\pi^-\eta$, $\eta \rightarrow \gamma\gamma$

For this decay mode two photons, reconstructing an η , and two tracks must be observed in the detector.

$\eta_c \rightarrow \text{K}^+\text{K}^-\pi^0$

For this decay mode two photons, reconstructing a π^0 , and two tracks must be observed in the detector. Since there exists no background from $\eta_c \rightarrow \pi^+\pi^-\pi^0$, only a loose cut on the dE/dx is used in order to keep the efficiency high: the K^+K^- probability divided by the sum of the K^+K^- and $\pi^+\pi^-$ probabilities must be larger than 30%.

$\eta_c \rightarrow \rho^+\rho^-$, $\rho^\pm \rightarrow \pi^\pm\pi^0$

Four photons are combined in order to find two π^0 candidates, which are combined with the two tracks to form two charged ρ mesons. The event is accepted if both combinations satisfy $|M(\pi^\pm\pi^0) - M(\rho^\pm)| < 0.25$ GeV.

$$\underline{\eta_c \rightarrow \pi^+\pi^-\eta, \eta \rightarrow \pi^+\pi^-\pi^0}$$

For this decay mode the cut on the angle between the two photons is widened to $\cos\psi_{\gamma\gamma} > 0.4$. Two out of the four observed tracks must combine with the π^0 candidate to form an η , with $|M(\pi^+\pi^-\pi^0) - M(\eta)| < 40$ MeV.

$$\underline{\eta_c \rightarrow \pi^+\pi^-\eta', \eta' \rightarrow \pi^+\pi^-\eta, \eta \rightarrow \gamma\gamma}$$

For this decay mode two photons, reconstructing an η , and four tracks must be observed in the detector. The η candidate must combine with two of the tracks to form an η' , with $|M(\pi^+\pi^-\eta) - M(\eta')| < 50$ MeV.

$$\underline{\eta_c \rightarrow \pi^+\pi^-\eta', \eta' \rightarrow \rho^0\gamma, \rho^0 \rightarrow \pi^+\pi^-}$$

To select this decay mode, ρ^0 candidates, formed by a pair of tracks with $0.60 \text{ GeV} < M(\pi^+\pi^-) < 0.92 \text{ GeV}$, are combined with a photon, with energy greater than 100 MeV, to form an η' , with $|M(\rho^0\gamma) - M(\eta')| < 60$ MeV and $\cos\psi_{\rho^0\gamma} > -0.3$.

The selection efficiencies for the analysed decay modes are given in Table 1, for both data samples at $\sqrt{s} \simeq 91$ GeV and at $\sqrt{s} \simeq 183$ GeV.

The mass distribution of the selected untagged events is presented in Figure 2. A fit of this spectrum in the mass range $2.4 \text{ GeV} < M < 3.2 \text{ GeV}$, with an exponential background plus a Gaussian for the signal, gives for the peak position $M(\eta_c) = 2.974 \pm 0.018$ GeV, in excellent agreement with the world average 2.979 ± 0.002 GeV [9]. The width of the Gaussian is 57 ± 16 MeV, consistent with the reconstructed width in the Monte Carlo of 70 MeV. The area of the peak corresponds to a total of 93 ± 33 η_c events.

The $\chi_{c0}(3417)$ and $\chi_{c2}(3556)$ are also known to decay into $\pi^+\pi^-\pi^+\pi^-$ and $K^+K^-\pi^+\pi^-$. Their branching ratios to the other analysed decay modes are unknown. Therefore the mass spectrum has been divided into two parts in Figure 3: Figure 3a shows the mass distribution of the events with one or more photons or a K_s^0 in the final state, while Figure 3b shows the mass spectrum of the $\pi^+\pi^-\pi^+\pi^-$ and $K^+K^-\pi^+\pi^-$ events. However, in Figure 3b, no enhancements are visible around the χ_{c0} and χ_{c2} masses. In Figure 3a, on the other hand, an enhancement is visible around 3.4 GeV. A fit to this enhancement in the mass range $3.2 \text{ GeV} < M < 4 \text{ GeV}$ gives for the peak position 3.400 ± 0.019 GeV, in agreement with the world average χ_{c0} mass $M(\chi_{c0}) = 3.417 \pm 0.003$ GeV, and for the width 58 ± 18 MeV, in agreement with the reconstructed width from the Monte Carlo of 70 MeV. The area of the fitted Gaussian is 29 ± 11 events. A similar fit to Figure 3b yields only 7 ± 6 events above background.

The two-photon width

Since the η_c signal has low statistics in each decay mode, the two-photon width is obtained with a combined unbinned likelihood fit. The fit takes into account the different weight of each decay mode due to the different background levels, efficiencies, branching ratios, and the different integrated luminosities at $\sqrt{s} \simeq 91$ GeV and at $\sqrt{s} \simeq 183$ GeV. All mass spectra are fitted simultaneously with a sum of a normalised exponential background function $b_i(x)$ and a Gaussian distribution $g_i(x)$, where i runs over the different decay modes and the two centre-of-mass energies considered:

$$f_i(x) = (1 - p_i)b_i(x) + p_i g_i(x). \quad (5)$$

Here, p_i is the ratio of the number of signal events, S_i , over the total number of events in mass spectrum i . The exponential background, $b_i(x)$, is allowed to vary for each spectrum, but the

number of signal events in the Gaussian for each spectrum is related to the two-photon width by

$$S_i = \epsilon_i \mathcal{L} \text{BR}_i \kappa \Gamma_{\gamma\gamma}. \quad (6)$$

Here, ϵ_i is the total efficiency, \mathcal{L} is the integrated luminosity, and BR_i is the branching ratio for decay mode i . The proportionality factor κ is obtained from Monte Carlo, using Equation (3). The events in χ_{c0} signal region (between 3.3 and 3.5 GeV) are excluded from the fit. For the $\text{K}^+\text{K}^-\pi^+\pi^-$ and $\pi^+\pi^-\pi^+\pi^-$ mass spectra, the whole region $M > 3.2$ GeV is excluded, where the χ_{c0} signal, the χ_{c2} signal, and small enhancements due to π/K misidentification are expected. The effect of this cut is taken into account in the systematic error. The η_c two-photon width obtained from the fit is 6.9 ± 1.7 (stat.) keV. It corresponds to a total of 76 ± 19 η_c events, in agreement with the number of events obtained with the fit to the total mass spectrum shown in Figure 2. The two-photon widths or upper limits for the individual decay modes are also given in Table 1. They have been obtained with an unbinned likelihood fit to the individual spectra using an exponential background and a Gaussian for the signal, with the Gaussian position and width fixed to the Monte Carlo values.

The systematic error related to the selection requirements includes contributions from the cut on the number of hits on a track (5%), from the dE/dx cuts (3%), and from the π^0 selection (4%). Furthermore, the systematic errors take into account uncertainties on the trigger efficiency (2%), on the Monte Carlo statistics (2%), on the background subtraction (3%) and on the uncertainty on the individual branching ratios (9%). They add up to 12%, resulting in a systematic error on $\Gamma_{\gamma\gamma}(\eta_c)$ of 0.8 keV. The uncertainty introduced by the poor knowledge of the branching ratio $\text{BR}(J \rightarrow \eta_c \gamma) = (1.27 \pm 0.36) \%$ [15], which is contained in all branching ratio uncertainties, leads to an additional error on $\Gamma_{\gamma\gamma}(\eta_c)$ of 2.0 keV.

In Table 2 our measurement is compared to previous measurements [8, 16] of the η_c two-photon width. It is found to be in good agreement. The measurement is also in good agreement with the theoretical predictions [5].

If we assume that the excess of events at 3.4 GeV is due to χ_{c0} formation, the χ_{c0} two-photon width can be obtained using a similar fit as for the η_c . However, only the $\pi^+\pi^-\pi^+\pi^-$ and $\text{K}^+\text{K}^-\pi^+\pi^-$ events, for which the χ_{c0} branching ratios are known, can be included in the fit. Since the number of signal events is low for these decay modes, it is only possible to set a 95% C.L. upper limit $\Gamma_{\gamma\gamma}(\chi_{c0}) < 5.5$ keV. This is consistent with the upper limit by CLEO, $\Gamma_{\gamma\gamma}(\chi_{c0}) < 6.2$ keV, and the measurement by the Crystal Ball experiment, $\Gamma_{\gamma\gamma}(\chi_{c0}) = 4.0 \pm 2.8$ keV [17].

Also the $\chi_{c2}(3556)$ has known branching ratios into $\pi^+\pi^-\pi^+\pi^-$ and $\text{K}^+\text{K}^-\pi^+\pi^-$. No signal is observed in Figure 3b. We obtain for the χ_{c2} two-photon width a 95% C.L. upper limit of 1.4 keV, consistent with our previous measurement [18].

We also observe no signal for the $\eta'_c(3594)$. Reference [19] predicts the hadronic branching ratios of the η_c and η'_c to be about equal. If we assume that the efficiencies and branching ratios of the η'_c are the same as for the η_c for the analysed final states, we obtain $\Gamma_{\gamma\gamma}(\eta'_c) < 2.0$ keV at 95% C.L.

The η_c form factor

The η_c transition form factor, as defined in Equation (2), can be studied using tagged events. The mass spectrum of the events with an electron found in the LUMI at $\sqrt{s} \simeq 91$ GeV or in the VSAT at $\sqrt{s} \simeq 183$ GeV is shown in Figure 4. The number of events with a tag in the

LUMI at $\sqrt{s} \simeq 183$ GeV is too low to contribute to the measurement. At $\sqrt{s} \simeq 91$ GeV, the LUMI covers the Q^2 range from 1.3 GeV² to 8.5 GeV². The VSAT covers at $\sqrt{s} \simeq 183$ GeV the Q^2 range between 0.2 GeV² and 0.8 GeV². The solid line in Figure 4 represents a fit with an exponential for the background and a Gaussian for the signal, with the position and width of the η_c Gaussian fixed to the Monte Carlo values. The area of the Gaussian is $8.3^{+5.5}_{-4.9}$ events.

We assume that the shape of the η_c form factor is described by the Vector Meson Dominance model form factor given in Equation (4). We compare three hypotheses for the pole mass Λ : a ρ -pole, which is found to be a good description of the Q^2 dependence of the π^0 , η , and η' cross sections [20], a J-pole, which is predicted to be a good approximation of the Q^2 dependence of the η_c cross section [6, 7], and an infinite pole or flat form factor, *i.e.* the $\gamma\gamma \rightarrow \eta_c$ cross section has no Q^2 dependence. Since our η_c Monte Carlo has been generated with a J-pole, the Monte Carlo events are reweighted to simulate a ρ -pole or flat form factor.

From Equations (1) and (2) it can be seen that the cross section is proportional to the product of the two-photon width and the form factor. In order to measure the form factor in a Q^2 -interval ΔQ^2 , the ratio $\sigma_{\text{data}}(\Delta Q^2)/\Gamma_{\gamma\gamma}$ has to be determined. The two-photon width $\Gamma_{\gamma\gamma}$ has already been measured using untagged events, and the cross section $\sigma_{\text{data}}(\Delta Q^2)$ can be obtained using the tagged events. Note that in the ratio $\sigma_{\text{data}}(\Delta Q^2)/\Gamma_{\gamma\gamma}$ almost all systematic errors cancel, in particular the error due to the uncertainty in $\text{BR}(J \rightarrow \eta_c\gamma)$.

The two cross sections $\sigma_{\text{data}}(\Delta Q^2)$, for events with a tag in the LUMI and for events with a tag in the VSAT, are obtained using an unbinned likelihood fit. The fit is similar to the one used to obtain the two-photon width, with the number of tagged signal events in each spectrum, S_i , equal to $\epsilon_i(\Delta Q^2) \mathcal{L} \text{BR}_i \sigma_{\text{data}}(\Delta Q^2)$. The efficiencies per Q^2 interval, $\epsilon_i(\Delta Q^2)$, have an uncertainty due to the choice of the form factor in the Monte Carlo less than 3%. The cross sections correspond to 7.7 ± 3.0 events with a tag in the LUMI and 2.3 ± 2.3 events with a tag in the VSAT.

The $\sigma_{\text{data}}(\Delta Q^2)/\Gamma_{\gamma\gamma}$ ratios are given in Table 3, together with the Monte Carlo predictions for the three form factor hypotheses. A χ^2 representing how well the measured $\sigma_{\text{data}}(\Delta Q^2)/\Gamma_{\gamma\gamma}$ correspond to the Monte Carlo predictions is calculated and the corresponding probabilities are given in the last column of Table 3 for each form factor hypothesis. The changes in the χ^2 probabilities due to the variation of $\Gamma_{\gamma\gamma}$ within its measured error (± 1.7 keV) are given in parentheses in the last column. The J-pole form factor and the flat form factor are clearly favoured over the ρ -pole form factor.

Since $\sigma(\Delta Q^2)$ is proportional to $F^2(Q^2)$, the latter can be obtained by dividing the measured cross section (normalised to the measured two-photon width) by the Monte Carlo cross section with a flat form factor, for which $F^2 = 1$,

$$F^2(Q^2) = \frac{\sigma_{\text{data}}(\Delta Q^2)}{\sigma_{\text{flat MC}}(\Delta Q^2)}. \quad (7)$$

The $F^2(Q^2)$ measured in the two Q^2 intervals is shown in Figure 5, together with three curves corresponding to the theoretical predictions for a ρ -pole, J-pole and flat form factor. For a J-pole Monte Carlo, the average Q^2 for events with a tag in the LUMI is 3.08 GeV², and for events with a tag in the VSAT it is 0.42 GeV². If the data are fitted with Equation (4) with the pole mass Λ left free, we obtain $\Lambda = 5.3^{+\infty}_{-2.5}$ GeV. The 95% confidence level lower limit on the pole mass is 1.6 GeV.

Conclusions

The charmonium resonance η_c is observed through the reconstruction of nine different decay modes at $\sqrt{s} = 91$ GeV and at $\sqrt{s} = 183$ GeV. The two-photon width is determined to be $\Gamma_{\gamma\gamma}(\eta_c) = 6.9 \pm 1.7$ (stat.) ± 0.8 (sys.) ± 2.0 (BR) keV, in agreement with earlier measurements. This corresponds to 76 ± 19 signal events in total. A χ_{c0} signal of 29 ± 11 events is also observed, but $\Gamma_{\gamma\gamma}(\chi_{c0})$ cannot be evaluated since its branching ratios are unknown. We find upper limits $\Gamma_{\gamma\gamma}(\chi_{c0}) < 5.5$ keV, $\Gamma_{\gamma\gamma}(\chi_{c2}) < 1.4$ keV, and $\Gamma_{\gamma\gamma}(\eta'_c) < 2.0$ keV. Using tagged η_c events we establish that the Q^2 dependence of the cross section is better described by a J-mass pole in the Vector Meson Dominance form factor than by a ρ -mass pole.

Acknowledgements

We wish to express our gratitude to the CERN accelerator division for the excellent performance of the LEP machine. We acknowledge the contributions of the engineers and technicians who have participated in the construction and maintenance of this experiment.

Author List

The L3 Collaboration:

M.Acciarri²⁵ P.Achard¹⁸ O.Adriani¹⁵ M.Aguilar-Benitez²⁴ J.Alcaraz²⁴ G.Alemanni²¹ J.Allaby¹⁶ A.Aloisio²⁷
M.G.Alvigi²⁷ G.Ambrosi¹⁸ H.Anderhub⁴⁶ V.P.Andreev^{6,35} T.Angelescu² F.Anselmo⁹ A.Arefiev²⁶ T.Azmoon³
T.Aziz¹⁰ P.Bagnaia³⁴ L.Baksay⁴¹ A.Balandras⁴ R.C.Ball³ S.Banerjee¹⁰ Sw.Banerjee¹⁰ A.Barczyk^{46,44}
R.Barillère¹⁶ L.Barone³⁴ P.Bartalini²¹ M.Basile⁹ R.Battiston³¹ A.Bay²¹ F.Becattini¹⁵ U.Becker¹⁴ F.Behner⁴⁶
J.Berdugo²⁴ P.Berges¹⁴ B.Bertucci³¹ B.L.Betev⁴⁶ S.Bhattacharya¹⁰ M.Biasini³¹ A.Biland⁴⁶ J.J.Blaising⁴
S.C.Blyth³² G.J.Bobbink² A.Böhm¹ L.Boldizsar¹³ B.Borgia³⁴ D.Bourilkov⁴⁶ M.Bourquin¹⁸ S.Braccini¹⁸
J.G.Branson³⁷ V.Brigljevic⁴⁶ F.Brochu⁴ A.Buffini¹⁵ A.Buijs⁴² J.D.Burger¹⁴ W.J.Burger³¹ J.Busenitz⁴¹
A.Button³ X.D.Cai¹⁴ M.Campanelli⁴⁶ M.Capell¹⁴ G.Cara Romeo⁹ G.Carlino²⁷ A.M.Cartacci¹⁵ J.Casaus²⁴
G.Castellini¹⁵ F.Cavallari³⁴ N.Cavallo²⁷ C.Cecchi¹⁸ M.Cerrada⁴ F.Cesaroni²² M.Chamizo¹⁸ Y.H.Chang⁴⁸
U.K.Chaturvedi¹⁷ M.Chemarin²³ A.Chen⁴⁸ G.Chen⁷ G.M.Chen⁷ H.F.Chen¹⁹ H.S.Chen⁷ X.Chereau⁴ G.Chiefari²⁷
L.Cifarelli³⁶ F.Cindolo⁹ C.Civinini¹⁵ I.Clare¹⁴ R.Clare¹⁴ G.Coignet⁴ A.P.Colijn² N.Colino²⁴ S.Costantini⁸
F.Cotorobai¹² B.Cozzoni⁹ B.de la Cruz²⁴ A.Csilling¹³ S.Cucciarelli³¹ T.S.Dai⁴ J.A.van Dalen²⁹
R.D'Alessandro¹⁵ R.de Asmundis²⁷ P.Deglon¹⁸ A.Degré⁴ K.Deiters⁴⁴ D.della Volpe²⁷ P.Denes³³
F.DeNotaristefani³⁴ A.De Salvo⁴⁶ M.Diemoz³⁴ D.van Dierendonck² F.Di Lodovico⁴⁶ C.Dionisi³⁴ M.Dittmar⁴⁶
A.Dominguez³⁷ A.Doria²⁷ M.T.Dova^{17,‡} D.Duchesneau⁴ D.Dufournand⁴ P.Duinker² I.Duran³⁸ H.El Mamouni²³
A.Engler³² F.J.Eppling¹⁴ F.C.Erné² P.Extermann¹⁸ M.Fabre⁴⁴ R.Faccini³⁴ M.A.Falagan²⁴ S.Falciano^{34,16}
A.Favara¹⁶ J.Fay²³ O.Fedin³⁵ M.Felcini⁴⁶ T.Ferguson³² F.Ferroni³⁴ H.Fesefeldt¹ E.Fiandrini³¹ J.H.Field¹⁸
F.Filthaut¹⁶ P.H.Fisher¹⁴ I.Fisk³⁷ G.Forconi¹⁴ L.Fredj¹⁸ K.Freudenreich⁴⁶ C.Furetta²⁵ Yu.Galaktionov^{26,14}
S.N.Ganguli¹⁰ P.Garcia-Abia⁵ M.Gataullin³⁰ S.S.Gau¹¹ S.Gentile^{34,16} N.Gheordanescu¹² S.Giagu³⁴ Z.F.Gong¹⁹
G.Grenier²³ O.Grimm⁴⁶ M.W.Gruenewald⁸ R.van Gulik² V.K.Gupta³³ A.Gurtu¹⁰ L.J.Gutay⁴³ D.Haas⁵
A.Hasan²⁸ D.Hatzifotiadou⁹ T.Hebbeker⁸ A.Hervé¹⁶ P.Hidas¹³ J.Hirschfelder³² H.Hofer⁴⁶ G.Holzner⁴⁶
H.Hoorani³² S.R.Hou⁴⁸ I.Iashvili⁴⁵ B.N.Jin⁷ L.W.Jones³ P.de Jong² I.Josa-Mutuberria²⁴ R.A.Khan¹⁷
D.Kamrad⁴⁵ M.Kaur^{17,◇} M.N.Kienzle-Focacci¹⁸ D.Kim³⁴ D.H.Kim⁴⁰ J.K.Kim⁴⁰ S.C.Kim⁴⁰ J.Kirkby¹⁶ D.Kiss¹³
W.Kittel²⁹ A.Klimentov^{14,26} A.C.König²⁹ A.Kopp⁴⁵ I.Korolko²⁶ V.Koutsenko^{14,26} M.Kräber⁴⁶ R.W.Kraemer³²
W.Krenz¹ A.Kunin^{14,26} P.Lacetre^{45,‡,‡} P.Ladron de Guevara²⁴ I.Laktinel²³ G.Landi¹⁵ K.Lassila-Perini⁴⁶
P.Laurikainen²⁰ A.Lavorato³⁶ M.Lebeau¹⁶ A.Lebedev¹⁴ P.Lebrun²³ P.Lecomte⁴⁶ P.Lecoq¹⁶ P.Le Coultre⁴⁶
H.J.Lee⁸ J.M.Le Goff¹⁶ R.Leiste⁴⁵ E.Leonardi³⁴ P.Levtchenko³⁵ C.Li¹⁹ C.H.Lin⁴⁸ W.T.Lin⁴⁸ F.L.Linde²
L.Lista²⁷ Z.A.Liu⁷ W.Lohmann⁴⁵ E.Longo³⁴ Y.S.Lu⁷ K.Lübelsmeyer¹ C.Luci^{16,34} D.Luckey¹⁴ L.Lugnier²³
P.Luminari³⁴ W.Lustermann⁴⁶ W.G.Ma¹⁹ M.Maity¹⁰ L.Malgeri¹⁶ A.Malinin^{26,16} C.Maña²⁴ D.Mangeol²⁹
L.Marchesini⁴⁶ G.Marian^{41,¶} J.P.Martin²³ F.Marzano³⁴ G.G.G.Massaro² K.Mazumdar¹⁰ R.R.McNeil⁶ S.Mele¹⁶
L.Merola²⁷ M.Meschini¹⁵ W.J.Metzger²⁹ M.von der Mey¹ D.Migani⁹ A.Mihul¹² H.Milcent¹⁶ G.Mirabella³⁴
J.Mnich¹⁶ G.B.Mohanty¹⁰ P.Molnar⁸ B.Monteleoni¹⁵ T.Moulik¹⁰ G.S.Muanza²³ F.Muheim¹⁸ A.J.M.Muijs²
M.Napolitano²⁷ F.Nessi-Tedaldi⁴⁶ H.Newman³⁰ T.Niessen¹ A.Nisati³⁴ H.Nowak⁴⁵ Y.D.Oh⁴⁰ G.Organtini³⁴
R.Ostonen²⁰ C.Palomares²⁴ D.Pandoulas¹ S.Paoletti^{34,16} P.Paolucci²⁷ H.K.Park³² I.H.Park⁴⁰ G.Pascale³⁴
G.Passaleva¹⁶ S.Patricelli²⁷ T.Paul¹¹ M.Pauluzzi³¹ C.Paus¹⁶ F.Pauss⁴⁶ D.Peach¹⁶ M.Pedace³⁴ Y.J.Pei¹
S.Pensotti²⁵ D.Perret-Gallix⁴ B.Petersen²⁹ D.Piccolo²⁷ M.Pieri¹⁵ P.A.Piroué³³ E.Pistoiesi²⁵ V.Plyaskin²⁶
M.Pohl⁴⁶ V.Pojidaev^{26,15} H.Postema¹⁴ J.Pothier¹⁶ N.Produit¹⁸ D.O.Prokofiev⁴³ D.Prokofiev³⁵ J.Quartieri³⁶
G.Rahal-Callot^{46,16} M.A.Rahaman¹⁰ N.Raja¹⁰ R.Ramelli⁴⁶ P.G.Rancoita²⁵ G.Raven³⁷ P.Razis²⁸ D.Ren⁴⁶
M.Rescigno³⁴ S.Reucroft¹¹ T.van Rhee⁴² S.Riemann⁴⁵ K.Riles³ A.Robohm⁴⁶ J.Rodin⁴¹ B.P.Roe³ L.Romero²⁴
A.Rosca⁸ S.Rosier-Lees⁴ J.A.Rubio¹⁶ D.Ruschmeier⁸ H.Ryckaczewski⁴⁶ S.Sarkar³⁴ J.Salicio¹⁶ E.Sanchez¹⁶
M.P.Sanders²⁹ M.E.Sarakinos²⁰ C.Schäfer¹ V.Schegelsky³⁵ S.Schmidt-Kaerst¹ D.Schmitz¹ H.Schopper⁴⁷
D.J.Schotanus²⁹ J.Schwenke¹ G.Schwering¹ C.Sciacca²⁷ D.Sciarrino¹⁸ A.Seganti⁹ L.Servoli³¹ S.Shevchenko³⁰
N.Shivarov³⁹ V.Shoutko²⁶ E.Shumilov²⁶ A.Shvorob³⁰ T.Siedenburg¹ D.Son⁴⁰ B.Smith³² P.Spillantini¹⁵
M.Steuer¹⁴ D.P.Stickland³³ A.Stone⁶ H.Stone³³ B.Stoyanov³⁹ A.Straessner¹ K.Sudhakar¹⁰ G.Sultanov¹⁷
L.Z.Sun¹⁹ H.Suter⁴⁶ J.D.Swain¹⁷ Z.Szillasi^{41,¶} X.W.Tang⁷ L.Tauscher⁵ L.Taylor¹¹ C.Timmermans²⁹
Samuel C.C.Ting¹⁴ S.M.Ting¹⁴ S.C.Tonwar¹⁰ J.Tóth¹³ C.Tully³³ K.L.Tung⁷ Y.Uchida¹⁴ J.Ulbricht⁴⁶ E.Valente³⁴
G.Vesztegombi¹³ I.Vetlitsky²⁶ D.Vicinanza³⁶ G.Viertel⁴⁶ S.Villa¹¹ M.Vivargent⁴ S.Vlachos⁵ I.Vodopianov³⁵
H.Vogel³² H.Vogt⁴⁵ I.Vorobiev²⁶ A.A.Vorobyov³⁵ A.Vorvolakos²⁸ M.Wadhwa⁵ W.Wallraff¹ M.Wang¹⁴
X.L.Wang¹⁹ Z.M.Wang¹⁹ A.Weber¹ M.Weber¹ P.Wienemann¹ H.Wilkens²⁹ S.X.Wu¹⁴ S.Wynhoff¹ L.Xia³⁰
Z.Z.Xu¹⁹ B.Z.Yang¹⁹ C.G.Yang⁷ H.J.Yang⁷ M.Yang⁷ J.B.Ye¹⁹ S.C.Yeh⁴⁹ J.M.You³² An.Zalite³⁵ Yu.Zalite³⁵
Z.P.Zhang¹⁹ G.Y.Zhu⁷ R.Y.Zhu³⁰ A.Zichichi^{9,16,17} F.Ziegler⁴⁵ G.Zilizi^{41,¶} M.Zöller¹

- 1 I. Physikalisches Institut, RWTH, D-52056 Aachen, FRG[§]
III. Physikalisches Institut, RWTH, D-52056 Aachen, FRG[§]
 - 2 National Institute for High Energy Physics, NIKHEF, and University of Amsterdam, NL-1009 DB Amsterdam, The Netherlands
 - 3 University of Michigan, Ann Arbor, MI 48109, USA
 - 4 Laboratoire d'Annecy-le-Vieux de Physique des Particules, LAPP, IN2P3-CNRS, BP 110, F-74941 Annecy-le-Vieux CEDEX, France
 - 5 Institute of Physics, University of Basel, CH-4056 Basel, Switzerland
 - 6 Louisiana State University, Baton Rouge, LA 70803, USA
 - 7 Institute of High Energy Physics, IHEP, 100039 Beijing, China[△]
 - 8 Humboldt University, D-10099 Berlin, FRG[§]
 - 9 University of Bologna and INFN-Sezione di Bologna, I-40126 Bologna, Italy
 - 10 Tata Institute of Fundamental Research, Bombay 400 005, India
 - 11 Northeastern University, Boston, MA 02115, USA
 - 12 Institute of Atomic Physics and University of Bucharest, R-76900 Bucharest, Romania
 - 13 Central Research Institute for Physics of the Hungarian Academy of Sciences, H-1525 Budapest 114, Hungary[‡]
 - 14 Massachusetts Institute of Technology, Cambridge, MA 02139, USA
 - 15 INFN Sezione di Firenze and University of Florence, I-50125 Florence, Italy
 - 16 European Laboratory for Particle Physics, CERN, CH-1211 Geneva 23, Switzerland
 - 17 World Laboratory, FBLJA Project, CH-1211 Geneva 23, Switzerland
 - 18 University of Geneva, CH-1211 Geneva 4, Switzerland
 - 19 Chinese University of Science and Technology, USTC, Hefei, Anhui 230 029, China[△]
 - 20 SEFT, Research Institute for High Energy Physics, P.O. Box 9, SF-00014 Helsinki, Finland
 - 21 University of Lausanne, CH-1015 Lausanne, Switzerland
 - 22 INFN-Sezione di Lecce and Università Degli Studi di Lecce, I-73100 Lecce, Italy
 - 23 Institut de Physique Nucléaire de Lyon, IN2P3-CNRS, Université Claude Bernard, F-69622 Villeurbanne, France
 - 24 Centro de Investigaciones Energéticas, Medioambientales y Tecnológicas, CIEMAT, E-28040 Madrid, Spain^b
 - 25 INFN-Sezione di Milano, I-20133 Milan, Italy
 - 26 Institute of Theoretical and Experimental Physics, ITEP, Moscow, Russia
 - 27 INFN-Sezione di Napoli and University of Naples, I-80125 Naples, Italy
 - 28 Department of Natural Sciences, University of Cyprus, Nicosia, Cyprus
 - 29 University of Nijmegen and NIKHEF, NL-6525 ED Nijmegen, The Netherlands
 - 30 California Institute of Technology, Pasadena, CA 91125, USA
 - 31 INFN-Sezione di Perugia and Università Degli Studi di Perugia, I-06100 Perugia, Italy
 - 32 Carnegie Mellon University, Pittsburgh, PA 15213, USA
 - 33 Princeton University, Princeton, NJ 08544, USA
 - 34 INFN-Sezione di Roma and University of Rome, "La Sapienza", I-00185 Rome, Italy
 - 35 Nuclear Physics Institute, St. Petersburg, Russia
 - 36 University and INFN, Salerno, I-84100 Salerno, Italy
 - 37 University of California, San Diego, CA 92093, USA
 - 38 Dept. de Física de Partículas Elementales, Univ. de Santiago, E-15706 Santiago de Compostela, Spain
 - 39 Bulgarian Academy of Sciences, Central Lab. of Mechatronics and Instrumentation, BU-1113 Sofia, Bulgaria
 - 40 Center for High Energy Physics, Adv. Inst. of Sciences and Technology, 305-701 Taejeon, Republic of Korea
 - 41 University of Alabama, Tuscaloosa, AL 35486, USA
 - 42 Utrecht University and NIKHEF, NL-3584 CB Utrecht, The Netherlands
 - 43 Purdue University, West Lafayette, IN 47907, USA
 - 44 Paul Scherrer Institut, PSI, CH-5232 Villigen, Switzerland
 - 45 DESY-Institut für Hochenergiephysik, D-15738 Zeuthen, FRG
 - 46 Eidgenössische Technische Hochschule, ETH Zürich, CH-8093 Zürich, Switzerland
 - 47 University of Hamburg, D-22761 Hamburg, FRG
 - 48 National Central University, Chung-Li, Taiwan, China
 - 49 Department of Physics, National Tsing Hua University, Taiwan, China
- § Supported by the German Bundesministerium für Bildung, Wissenschaft, Forschung und Technologie
- ‡ Supported by the Hungarian OTKA fund under contract numbers T019181, F023259 and T024011.
- ¶ Also supported by the Hungarian OTKA fund under contract numbers T22238 and T026178.
- ^b Supported also by the Comisión Interministerial de Ciencia y Tecnología.
- [#] Also supported by CONICET and Universidad Nacional de La Plata, CC 67, 1900 La Plata, Argentina.
- [‡] Supported by Deutscher Akademischer Austauschdienst.
- ◇ Also supported by Panjab University, Chandigarh-160014, India.
- △ Supported by the National Natural Science Foundation of China.

References

- [1] V.M. Budnev *et al.*, Phys. Rep. **15** (1974) 181
- [2] L.D. Landau, Dokl. Akad. Nauk. USSR **60** (1948) 207;
C.N. Yang, Phys. Rev. **77** (1950) 242
- [3] Crystal Ball Collab., C. Edwards *et al.*, Phys. Rev. Lett. **48** (1982) 70
- [4] Delphi Collab., P. Abreu *et al.*, Phys. Lett. **B 441** (1998) 479
- [5] E.S. Ackleh and T. Barnes, Phys. Rev. **D45** (1992) 232;
T. Barnes, in “Proceedings of the IXth workshop on photon-photon collisions”, World Scientific (1992), p. 263;
M.R. Ahmady and R.R. Mendel, Phys. Rev. **D51** (1995) 141;
C.R. Münz, Nucl. Phys. **A609** (1996) 364;
H.-W. Huang *et al.*, Phys. Rev. **D 56** (1997) 368
- [6] Th. Feldmann and P. Kroll, Phys. Lett. **B 413** (1997) 410
- [7] G.A. Schuler, F.A. Berends, and R. van Gulik, Nucl. Phys. **B 523** (1998) 423
- [8] L3 Collab., O. Adriani *et al.*, Phys. Lett. **B 318** (1993) 575
- [9] Particle Data Group, C. Caso *et al.*, Eur. Phys. J. **C3** (1998) 1
- [10] L3 Collab., B. Adeva *et al.*, Nucl. Inst. Meth. **A 289** (1990) 35;
M. Chemarin *et al.*, Nucl. Inst. Meth. **A 349** (1994) 345;
M. Acciarri *et al.*, Nucl. Inst. Meth. **A 351** (1994) 300;
G. Basti *et al.*, Nucl. Inst. Meth. **A 374** (1996) 293;
I.C. Brock *et al.*, Nucl. Inst. Meth. **A 381** (1996) 236;
A. Adam *et al.*, Nucl. Inst. Meth. **A 383** (1996) 342
- [11] T. van Rhee, Ph.D. thesis in preparation, University of Utrecht
- [12] P. Béné *et al.*, Nucl. Inst. Meth. **A 306** (1991) 150
- [13] F.L. Linde, Ph.D. thesis, University of Leiden, 1988, unpublished
- [14] The L3 detector simulation is based on GEANT version 3.15.
See R. Brun *et al.*, “GEANT 3”, CERN DD/EE/84-1 (Revised), September 1987.
The GHEISHA program (H. Fesefeldt, RWTH Aachen Report PITHA 85/02 (1985)) is used to simulate hadronic interactions.
- [15] Crystal Ball Collab., Gaiser *et al.*, Phys. Rev. **D 34** (1986) 711
- [16] PLUTO Collab., Ch. Berger *et al.*, Phys. Lett. **B 167** (1986) 120;
TPC/2 γ Collab., H. Aihara *et al.*, Phys. Rev. Lett. **60** (1988) 2355;
CLEO Collab., W.-Y. Chen *et al.*, Phys. Lett. **B 243** (1990) 169;
ARGUS Collab., H. Albrecht *et al.*, Phys. Lett. **B 338** (1994) 390;
E760 Collab., T.A. Armstrong *et al.*, Phys. Rev. **D 52** (1995) 4839

- [17] CLEO Collab., Chen *et al.*, Phys. Lett. **B 243** (1990)169;
R.A. Lee (Crystal Ball Collab.), Ph.D. thesis, SLAC-Report-**282** (1985)
- [18] L3 Collab., M. Acciarri *et al.*, Phys. Lett. **B 453** (1999) 73
- [19] K.T. Chao, Y.F. Gu, and S.F. Tuan, ‘On Trigluonia in Charmonium Physics’, BIHEP-TH-93-45, PUTP-93-24, and UH-511-790-94 (1993);
S.F. Tuan, ‘Hadronic Decay Puzzle in Charmonium Physics’, UH-511-812-94 (1994), and
Proceedings of the 6th Annual Hadron Spectroscopy and Structure Colloquium (HSSC94),
Collega Park, Maryland, USA (1994)
- [20] TPC/2 γ Collab., H. Aihara *et al.*, Phys. Rev. Lett. **64** (1990) 172;
CELLO Collab., H.-J.Berends *et al.*, Z. Phys. **C49** (1991) 401;
L3 Collab., M. Acciarri *et al.*, Phys. Lett. **B 418** (1998) 399;
CLEO Collab., J. Gronberg *et al.*, Phys. Rev. **D57** (1998) 33.

Decay mode	BR(%)	ϵ_{91} (%)	ϵ_{183} (%)	$\Gamma_{\gamma\gamma}^{91}$ (keV)	$\Gamma_{\gamma\gamma}^{183}$ (keV)
$\eta_c \rightarrow \pi^+\pi^-\pi^+\pi^-$	1.2 ± 0.4	4.9	4.1	< 28	< 36
$\eta_c \rightarrow K^+K^-\pi^+\pi^-$	2.0 ± 0.7	5.2	4.5	10 ± 8	16 ± 10
$\eta_c \rightarrow K_s^0 K^\pm \pi^\mp$	1.3 ± 0.4	5.1	5.0	$5.4_{-3.4}^{+3.9}$	$5.5_{-3.9}^{+4.7}$
$\eta_c \rightarrow \pi^+\pi^-\eta(\gamma\gamma)$	1.3 ± 0.5	3.3	3.9	$7.4_{-4.4}^{+4.7}$	< 12
$\eta_c \rightarrow K^+K^-\pi^0$	0.9 ± 0.3	2.6	3.3	21_{-11}^{+12}	< 34
$\eta_c \rightarrow \rho^+\rho^-$	1.7 ± 0.6	0.8	0.9	< 28	24_{-17}^{+21}
$\eta_c \rightarrow \pi^+\pi^-\eta(\pi^+\pi^-\pi^0)$	0.8 ± 0.3	1.6	1.2	< 16	15_{-11}^{+18}
$\eta_c \rightarrow \pi^+\pi^-\eta'(\pi^+\pi^-\eta)$	0.5 ± 0.2	2.8	2.5	7_{-6}^{+7}	< 32
$\eta_c \rightarrow \pi^+\pi^-\eta'(\rho\gamma)$	0.8 ± 0.3	3.0	2.5	16 ± 10	< 29

Table 1: The branching ratio BR (derived from Reference [9]), the efficiencies $\epsilon_{\sqrt{s}}$, and the two-photon widths as obtained with an unbinned likelihood fit, at $\sqrt{s} \simeq 91$ GeV and $\sqrt{s} \simeq 183$ GeV for the different η_c decay modes considered in the analysis. All branching ratios contain a common error of 28% due to the uncertainty in BR($J \rightarrow \gamma\eta_c$).

Experiment	$\Gamma_{\gamma\gamma}(\eta_c)$ (keV)
PLUTO	28 ± 15
TPC/2 γ	$6.4_{-3.4}^{+5.0}$
CLEO	$5.9_{-1.8}^{+2.1} \pm 1.9$
L3	$8.0 \pm 2.4 \pm 2.3$
ARGUS	11.3 ± 4.2
E760	$6.7_{-1.7}^{+2.4} \pm 2.3$
L3 (this analysis)	$6.9 \pm 1.7 \pm 0.8 \pm 2.0$

Table 2: Summary of the published measurements of $\Gamma_{\gamma\gamma}(\eta_c)$ [8, 16].

	$\sigma(\Delta Q^2)/\Gamma_{\gamma\gamma}$ (pb/keV) LUMI	$\sigma(\Delta Q^2)/\Gamma_{\gamma\gamma}$ (pb/keV) VSAT	probability (%)
Data	1.3 ± 0.5	5 ± 5	
MC ρ -pole	0.051	0.81	4.3 (4.0 - 4.7)
MC J-pole	0.85	2.1	58 (34 - 81)
MC flat	1.6	2.3	70 (82 - 30)

Table 3: Results for the tagged η_c cross section $\sigma_{\text{data}}(\Delta Q^2)/\Gamma_{\gamma\gamma}(\eta_c)$ for events with a tag in the LUMI at $\sqrt{s} \simeq 91$ GeV and with a tag in the VSAT at $\sqrt{s} \simeq 183$ GeV, compared to the Monte Carlo predictions for a ρ -pole form factor, a J-pole form factor, and a flat form factor. In the last column the χ^2 probability that the data and the Monte Carlo are compatible is given for each form factor hypothesis. Between parentheses, the χ^2 probabilities if $\Gamma_{\gamma\gamma}$ is varied from 5.2 keV to 8.6 keV are given.

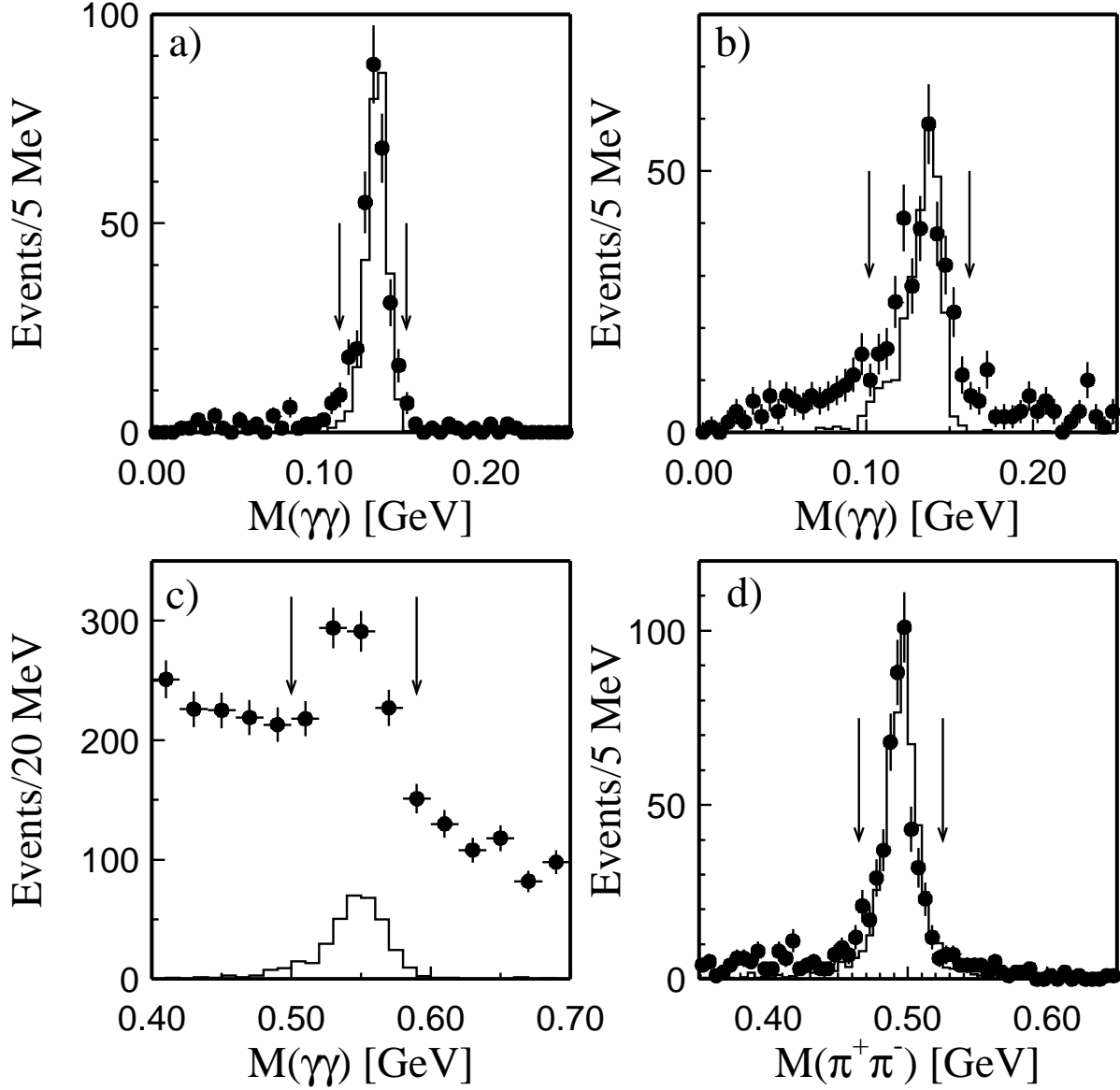


Figure 1: a) The invariant mass of two photons in the $K^+K^-\pi^0$ sample, with both photons in the barrel ($42^\circ < \theta < 138^\circ$) after all other cuts have been performed. The events between the arrows are accepted. b) The same, with at least one of the photons in the endcaps ($12^\circ < \theta < 38^\circ$ and $142^\circ < \theta < 168^\circ$). c) The invariant mass of two photons in the $\pi^+\pi^-\eta$ sample, after all other cuts have been performed. d) The invariant mass of the two tracks associated with a secondary vertex in the $K_s^0K^\pm\pi^\mp$ sample, selected with the cuts described in the text, after all other cuts have been made. In all plots the points with error bars represent the data, while the histogram represents the η_c Monte Carlo. The normalisation of the Monte Carlo is arbitrary.

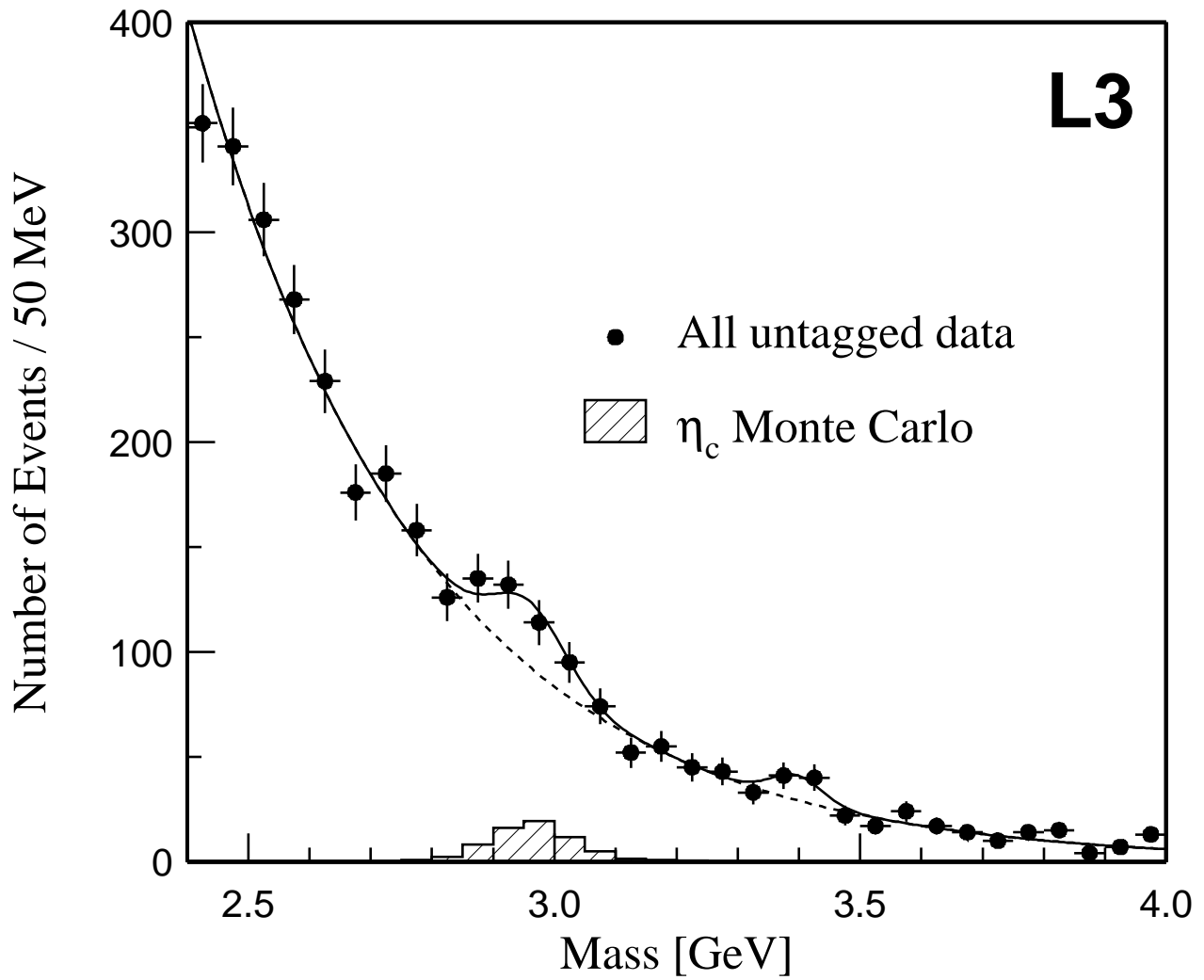


Figure 2: The mass distribution of all selected untagged events. The hatched histogram is the arbitrarily scaled η_c Monte Carlo. The solid lines represent a fit to the data with an exponential background and Gaussians for the η_c and χ_{c0} signals.

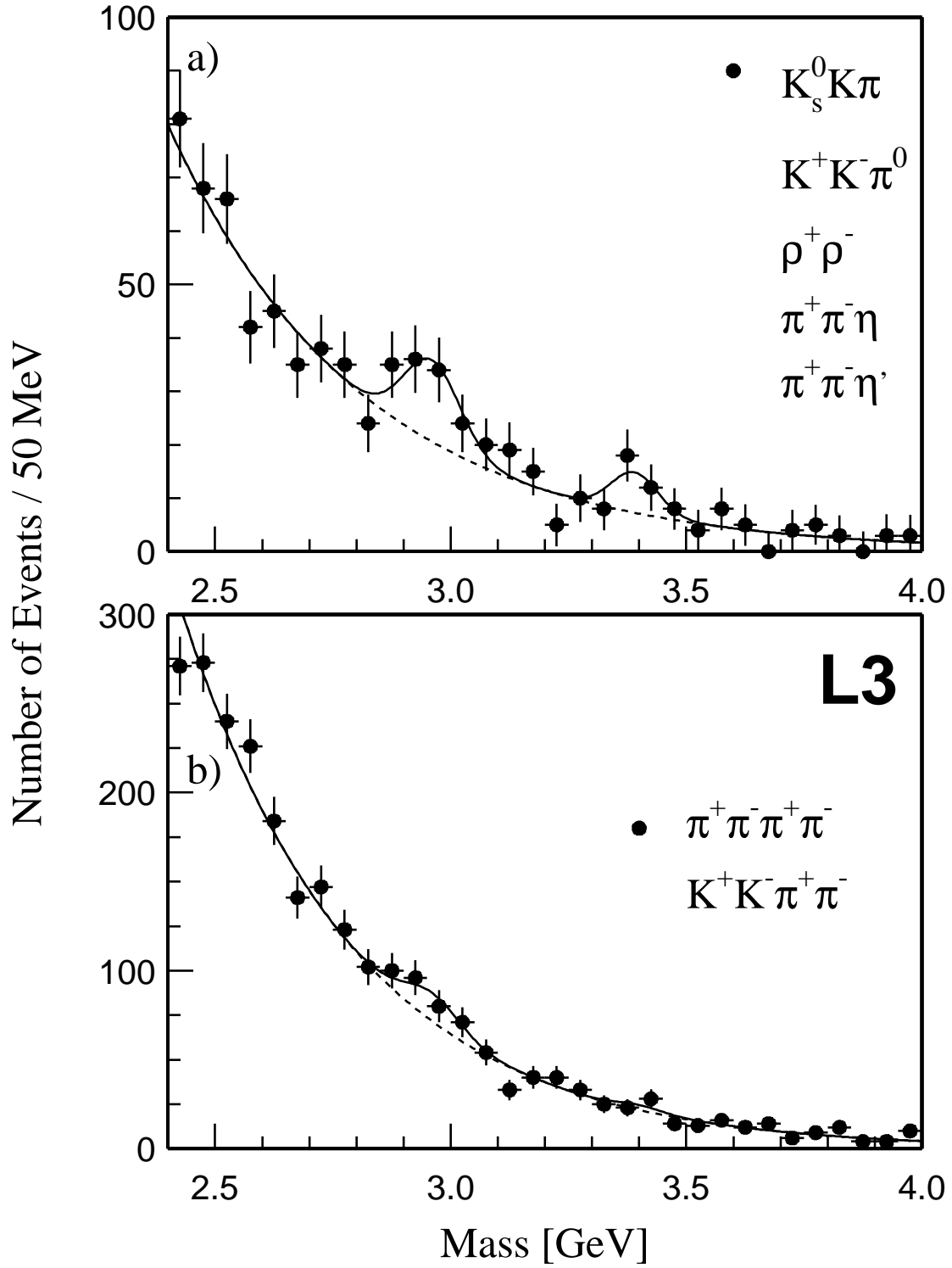


Figure 3: The mass distribution of the selected untagged events a) for the decay modes $K_s^0 K^\pm K^\mp$, $K^+ K^- \pi^0$, $\rho^+ \rho^-$, $\pi^+ \pi^- \eta$, and $\pi^+ \pi^- \eta'$, b) for the decay modes $\pi^+ \pi^- \pi^+ \pi^-$ and $K^+ K^- \pi^+ \pi^-$. The solid lines represent fits to the data with an exponential background and Gaussians for the η_c and χ_{c0} signals.

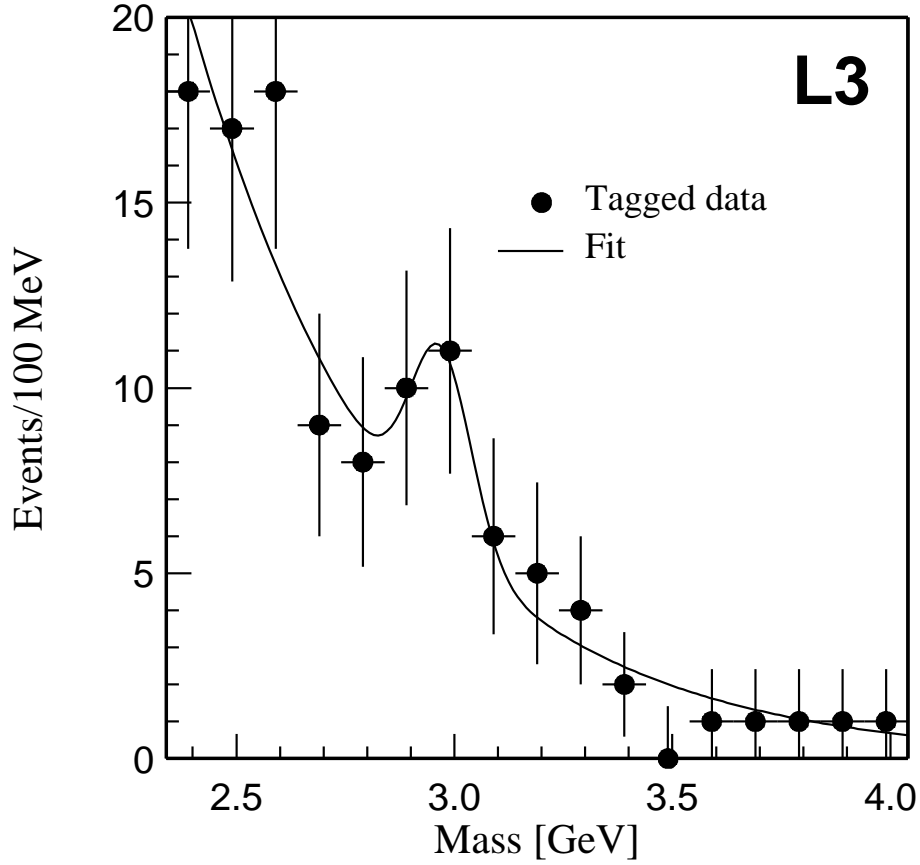


Figure 4: The mass distribution for selected events with a tag in the LUMI at $\sqrt{s} \simeq 91$ GeV, or with a tag in the VSAT at $\sqrt{s} \simeq 183$ GeV. The line is a fit with an exponential background and a Gaussian for the signal, with the mass and the width of the Gaussian fixed to the η_c Monte Carlo prediction.

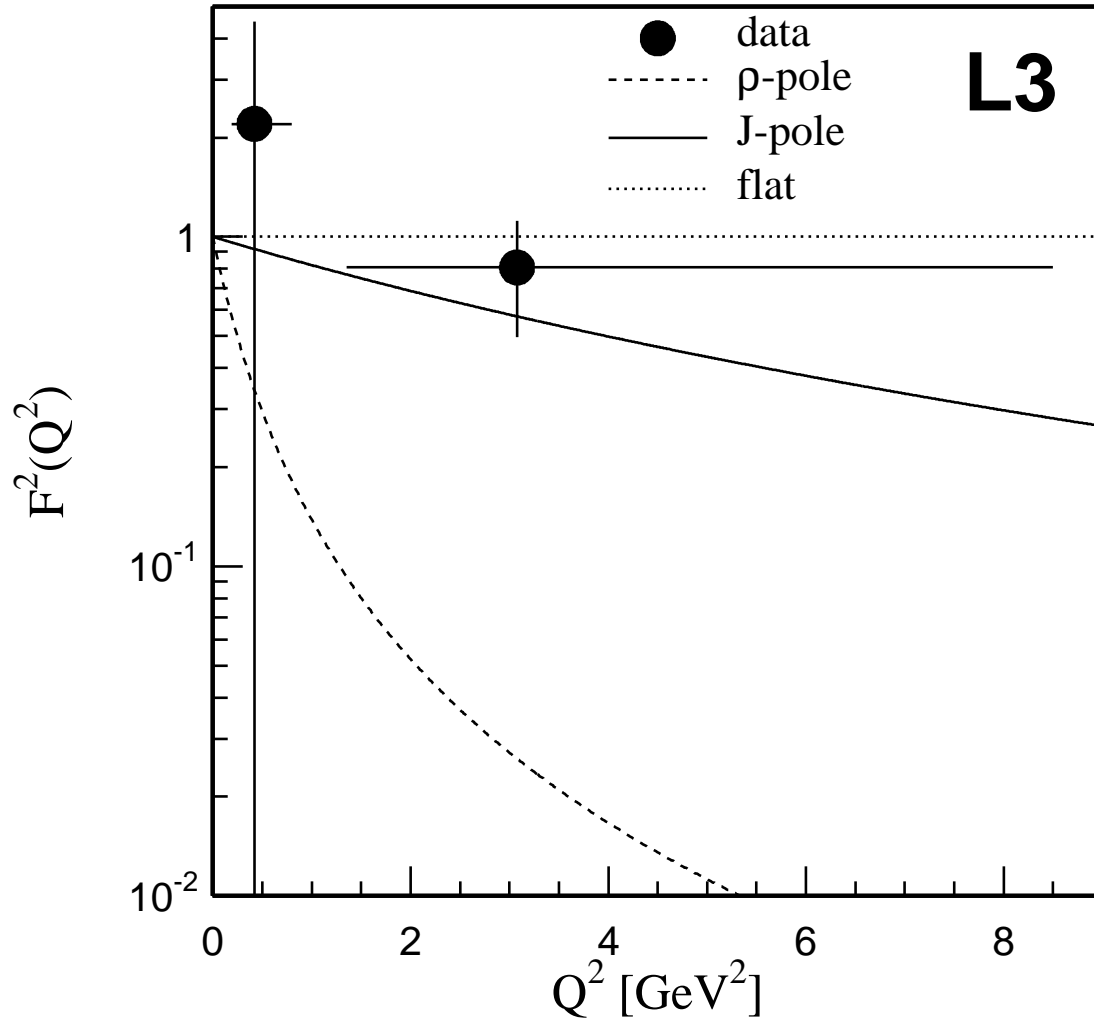


Figure 5: The form factor $F^2(Q^2)$ vs. Q^2 . The points represent the tagged data, while the three curves describe the form factor shape for a ρ -pole, J-pole or flat Monte Carlo.